Salting out the polar polymorph: Analysis by alchemical solvent transformation

Nathan Duff, Yuba Raj Dahal, Jeremy D. Schmit, and Baron Peters

Citation: The Journal of Chemical Physics **140**, 014501 (2014); doi: 10.1063/1.4853775
View online: http://dx.doi.org/10.1063/1.4853775
View Table of Contents: http://scitation.aip.org/content/aip/journal/jcp/140/1?ver=pdfcov
Published by the AIP Publishing

Salting out the polar polymorph: Analysis by alchemical solvent transformation

Nathan Duff,[1] Yuba Raj Dahal,[2] Jeremy D. Schmit,[2] and Baron Peters[3,4]
[1]*Chemical and Biomolecular Engineering, North Carolina State University, Raleigh, North Carolina 27695, USA*
[2]*Department of Physics, Kansas State University, Manhattan, Kansas 66506, USA*
[3]*Department of Chemical Engineering, University of California, Santa Barbara, California 93106, USA*
[4]*Department of Chemistry and Biochemistry, University of California, Santa Barbara, California 93106, USA*

(Received 8 September 2013; accepted 21 November 2013; published online 2 January 2014)

We computationally examine how adding NaCl to an aqueous solution with α- and γ-glycine nuclei alters the structure and interfacial energy of the nuclei. The polar γ-glycine nucleus in pure aqueous solution develops a melted layer of amorphous glycine around the nucleus. When NaCl is added, a double layer is formed that stabilizes the polar glycine polymorph and eliminates the surface melted layer. In contrast, the non-polar α-glycine nucleus is largely unaffected by the addition of NaCl. To quantify the stabilizing effect of NaCl on γ-glycine nuclei, we alchemically transform the aqueous glycine solution into a brine solution of glycine. The alchemical transformation is performed both with and without a nucleus in solution and for nuclei of α-glycine and γ-glycine polymorphs. The calculations show that adding 80 mg/ml NaCl reduces the interfacial free energy of a γ-glycine nucleus by 7.7 mJ/m^2 and increases the interfacial free energy of an α-glycine nucleus by 3.1 mJ/m^2. Both results are consistent with experimental reports on nucleation rates which suggest: $J(\alpha, \text{brine}) < J(\gamma, \text{brine}) < J(\alpha, \text{water})$. For γ-glycine nuclei, Debye-Hückel theory qualitatively, but not quantitatively, captures the effect of salt addition. Only the alchemical solvent transformation approach can predict the results for both polar and non-polar polymorphs. The results suggest a general "salting out" strategy for obtaining polar polymorphs and also a general approach to computationally estimate the effects of solvent additives on interfacial free energies for nucleation. © *2014 AIP Publishing LLC*. [http://dx.doi.org/10.1063/1.4853775]

I. INTRODUCTION

Solute precipitate nucleation is an important step in pharmaceutical crystallization,[1–5] biomineralization,[6–10] and self-assembly.[11–13] Different polymorphs, i.e., different crystal packings of the same compound, are known to differ in important properties like the crystal growth habit, the solubility, and rates of dissolution and growth.[2,4,5,14–16] Nucleation is key to controlling polymorphism and other properties because nucleation occurs before the later processes of growth, ripening, and agglomeration. Nucleation and polymorph selection depend not only on temperature and supersaturation, but also on more complex molecular level interactions and dynamics of the solute molecules, solvent molecules, and additives.

Ostwald[17] noted that unstable polymorphs tend to nucleate first from a supersaturated solution, with more stable polymorphs emerging from later polymorph transformations. However, changing the solvent, which does not alter relative polymorph stability, can alter polymorph selection.[18–21] Clearly, Ostwald's rule is not generally applicable. Stranski and Totomanov put forth the more general and fundamental view that activation free energy barriers control polymorph selection during nucleation.[22] Computing the free energy landscape for polymorph selection is feasible only for simple model systems,[23] so many investigators have sought more heuristic principles and methods for understanding and controlling polymorph selection. For example, in some cases, nucleation yields that polymorph in which the molecules retain their predominant solution phase conformation.[24–26] However, the dominant conformation in solution may also differ from conformations within the resulting polymorph.[27,28] Additionally, low concentration solvent additives can serve as molecular templates to promote nucleation and influence polymorph selection.[9,16,29–31]

Glycine polymorphism is widely studied both experimentally[32–38] and computationally.[39–44] Glycine is a small zwitterionic molecule with three polymorphs, γ-, α-, and β-glycine in decreasing order of stability, which can all be formed at ambient conditions. Thermodynamically stable γ-glycine (space group $P3_2$) is a polar polymorph of hexagonally packed glycine chains,[45] while α-glycine (space group $P2_1/n$) is sheets of hydrogen-bonded dimers,[46] and β-glycine is sheets of hydrogen-bonded monomers.[47] β-glycine nucleation and growth from aqueous solution requires a significant fraction of alcohol[48,49] or specialized additives, e.g., concentrated racemic phenylalanine,[50] so most studies of glycine nucleation and growth from aqueous solution focus on α- and γ-glycine. α-glycine forms first out of aqueous solution[37] while the thermodynamically stable γ-glycine forms first only out of aqueous solution with a variety of acids or bases,[36,38,45] inorganic salts,[36,37,51,52] or tailor made additives.[36,50]

Several theories have been proposed to explain how solvents and additives modulate polymorph selection between

α- and γ-glycine. The dimer hypothesis, put forth by Myerson and co-workers, was based on early evidence that centrosymmetric dimer units like those in the α-glycine structure are prevalent in aqueous solution. The prevalence of glycine dimers in solution was supported by diffusivities[34] and SAXS[32,33] measurements. The dimer structure is only present in α-glycine, not γ- or β-glycine, suggesting that prevalent dimers preferentially organize into α-glycine crystals. More recently Huang *et al.*[35] found that glycine monomers, and not dimers, are prevalent in aqueous solution based on freezing point depression and new self-diffusion measurements. Theoretical studies also suggest that glycine monomers are more common than dimers.[40,41,44] Furthermore, analysis of the structure of glycine pairs in solution indicates that catemers and not dimers are the most prevalent pair structure in aqueous solution.[40,41] Catemer units exist in the α-, β-, and γ-glycine polymorph structures. Therefore, the more recent studies suggest that dimers in aqueous solution cannot explain α-glycine polymorph selection in water.

Others have focused on understanding the additives that favor the formation of γ-glycine. The most common additives used to form γ-glycine are strong inorganic acids or bases, and inorganic salts.[36,37,51–53] γ-glycine can be obtained from pure aqueous solutions by thin film evaporation,[54] but this exception may be related to acidity of the air-water surface.[54,55] Several hypotheses for the mechanism by which these additives favor γ-glycine focus on the growth rates of α- and γ-glycine. Towler *et al.* hypothesized that acids and bases cause surface poisoning of the fast growing faces of α-glycine.[36] Towler *et al.* also proposed that inorganic ions like Na^+ can poison the fast growth of α-glycine and thereby favor γ-glycine in solution.[36] According to theories of crystal growth, additives that poison the growth of certain faces should increase the size of those faces in the crystal shape.[3] Indeed, NaCl, malonic acid (anionic glycine analog), and ethylenediamine (cationic glycine analog) additives do increase the size of fast growing α-glycine faces. However, Han *et al.* showed that polymorph selection was not consistently related to α- and γ-glycine growth rates in acid and base solutions.[38] Instead, Han *et al.* showed that the formation of α- and γ-glycine was determined by their relative nucleation rates in acidic and basic solution.[56] Of particular interest for the current work, Han *et al.* also found that the nucleation rate for γ-glycine in aqueous NaCl solution is slower than the nucleation rate of α-glycine in aqueous solution (without additives).[56]

According to the classical nucleation theory (CNT), the nucleation barrier originates from the interfacial free energy between the stable nucleus and the metastable solution. CNT gives the free energy to form a nucleus of size n as $F_{CNT}(n) = -n\Delta\mu + \gamma a n^{2/3}$ where $\Delta\mu$ is the chemical potential driving force, a is a shape-dependent area factor, and γ is the interfacial free energy between the nucleus and the solution.[57–59] At large nucleus sizes, the favorable bulk free energy dominates and nuclei grow. At small nucleus sizes, the interfacial term dominates and nuclei dissolve back into the bulk. At the critical size, $n^{\ddagger} = (2\gamma a/3\Delta\mu)^3$, the opposing forces which push the nucleus to grow or shrink are balanced in an unstable equilibrium. CNT predicts that the (homogeneous) nucleation rate J is approximately

$$J_{CNT} = A_{CNT} \exp\left[-\left(\frac{\gamma a}{k_B T}\right)^3 \frac{4}{27 \ln^2 S}\right], \qquad (1)$$

where A_{CNT} is a prefactor with units $m^{-3}\,s^{-1}$, S is the supersaturation, k_BT is the thermal energy, and $\Delta\mu = k_BT\,lnS$.[57] Concepts from CNT are central to most theories of homogeneous nucleation[58,59] and heterogeneous nucleation.[57] Recently even two-step nucleation was shown to emerge from slow diffusion transport in combination with the classical model.[60,61] Nucleation processes which are catalyzed by solvent additives share some characteristics of purely homogeneous and heterogenous nucleation mechanisms. Equation (1) shows how additives might catalyze nucleation by lowering interfacial free energies, similar to a heterogeneous surface that wets the nucleus. Moreover, additives that specifically increase or decrease the interfacial free energy of a specific polymorph might selectively suppress or promote, respectively, the nucleation of that polymorph.

Unfortunately, although CNT correctly predicts trends in the dependence on supersaturation and surface tension, it is not quantitatively accurate for absolute nucleation rates. A likely source of error is that CNT uses the interfacial tension γ of a macroscopic flat interface to describe nuclei with nanoscale radii.[62] Interfacial free energies of flat macroscopic interfaces can be measured[63] and computed.[64–67] However, interfacial free energies of macroscopic faces can differ substantially from the nanoscopic curved faces of nuclei. Therefore, a few methods for computing the interfacial free energy of small nuclei have also been developed. One approach involves fitting the free energy $F(n)$ from simulation data to the free energy $F_{CNT}(n)$ with the interfacial free energy γ as a fitting parameter.[68,69] Fitting to CNT is limited to single component nucleation processes (or multicomponent lattice models[70]) where $F(n)$ can be directly computed in atomistic simulations with importance sampling methods. Thus far, fitting $F_{CNT}(n)$ to atomistic simulation data for $F(n)$ has not been feasible for solute precipitate nucleation.

Two recent methods can directly estimate the interfacial free energy of solute nuclei in explicit solvents. Duff and Peters[71] proposed the Mitosis method that isolates the size dependent interfacial free energy by reversibly splitting a nucleus into two independent halves. Persson *et al.*[72] developed a thermodynamic cycle to calculate the free energy to form a cluster in solution. In principle either of these two methods could estimate the effects of an additive on the interfacial free energy by performing two calculations, one with additive and one without. This paper shows that additive effects on the interfacial free energy can be more directly probed by alchemically transforming the solvent around the nucleus. First, we develop the alchemical transformation approach. Second, we introduce simple electrostatics calculations to remove finite size effects associated with periodic boundary conditions. We then use the alchemical solvent transformation to compute the change in interfacial free energy for α- and γ-glycine nuclei upon addition of NaCl to an aqueous

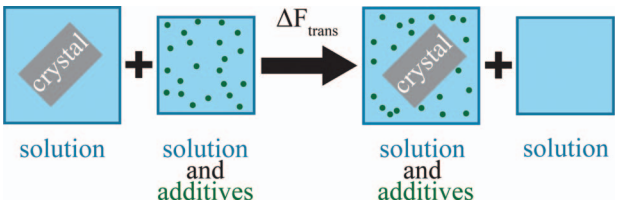

FIG. 1. Schematic of ΔF_{trans} calculation of the free energy to transfer a nucleus from one solvent to another.

supersaturated glycine solution. Finally, we compare to predictions of Debye-Hückel theory.

II. ALCHEMICAL SOLVENT TRANSFORMATION

The change in effective interfacial energy of a nucleus for the addition of an additive ($\Delta\gamma$) is computed from the free energy to transfer a nucleus from a simulation box without additive to one with additive (ΔF_{trans}). A schematic of the transfer process is shown in Fig. 1. The bulk additive-solvent interactions are conserved throughout the transformation. Therefore the change in free energy, ΔF_{trans} reflects only the new interactions between the nucleus and the new solvent. Normalizing ΔF_{trans} by the surface area (A) of the nucleus gives a change in the effective interfacial free energy for the addition of an additive:

$$\Delta\gamma = \Delta F_{trans}/A. \tag{2}$$

The $\Delta\gamma$ calculated here is an average of all of the crystal facets on the nucleus; therefore, this calculation is sensitive to the shape of the nucleus used.

Instead of calculating the free energy to remove a nucleus from solution and insert it into another solution with additives, we calculate the free energy to change the solution around the nucleus from one without additives to one with additives. In this approach, there are two simulation boxes: a simulation box of homogeneous solution and a simulation box containing a solvated nucleus. The amount of solution in each simulation box is equivalent. In this approach, ΔF_{trans} can equivalently be defined as

$$\Delta F_{trans} = \Delta F_{nuc} - \Delta F_{soln}, \tag{3}$$

where ΔF_{nuc} is the change in free energy associated with adding additive to solvent around the nucleus, and ΔF_{soln} is the change in free energy associated with adding additive to the simulation box with no nucleus. We calculate ΔF_{nuc} and ΔF_{soln} by alchemically transforming[73–75] a subset of solvent molecules into additive molecules. Alchemical transformations[73–75] use free energy perturbation theory[76] to transform one molecule into another through a series of nonphysical intermediate states. The approach is often used to calculate differences in solvation free energies[77] and differences in binding free energies between different molecules.[78]

Our calculations use a parameter λ that changes from 0 to 1 to turn some of the water molecules in solution into sodium and chloride ions to create a brine solvent. The force field parameters of the water-ion molecules as a function of λ are defined as follows:

$$\begin{aligned} q_k(\lambda) &= \lambda q_k^{(ion)} + (1-\lambda) q_k^{(water)}, \\ R_k(\lambda) &= \lambda R_k^{(ion)} + (1-\lambda) R_k^{(water)}, \\ \varepsilon_k(\lambda) &= \lambda \varepsilon_k^{(ion)} + (1-\lambda) \varepsilon_k^{(water)}. \end{aligned} \tag{4}$$

Here $q_k^{(X)}$, $R_k^{(X)}$, $\varepsilon_k^{(X)}$ are the charge, Lennard-Jones radius, and Lennard-Jones well depth on perturbed atom k of type X. For computational efficiency, solvent molecules should be transformed into additives, and where possible the insertion of new atoms should be avoided. In the current work, the TIP3P water[79] oxygen is transformed into a Cl^- or Na^+ ion while the hydrogen charges are annihilated. Since the hydrogen positions in the TIP3P water molecule lack Lennard-Jones interactions,[79] no insertion or deletion of Lennard-Jones interaction is required. For the remainder of this paper, the solvent at $\lambda = 0$ is referred to as water, and the solvent with $\lambda = 1$ is referred to as a brine solution. Both solutions also contain glycine molecules as discussed in Sec. IV.

The change in free energy for a transformation involving N stages of free energy perturbations is[80]

$$\Delta F = -k_B T \sum_{i=1}^{N} \ln\langle exp\{-\beta[H(\lambda_{i+1}) - H(\lambda_i)]\}\rangle_i, \tag{5}$$

where H is the Hamiltonian of the system with parameter λ_i, at state point i, and $\beta = 1/k_B T$. The exponential averages in Eq. (5) are calculated by using thermostatted and barostatted molecular dynamics (MD) to sample configurations according to Hamiltonian $H(\lambda_i)$, with $H(\lambda_i)$ and $H(\lambda_{i+1})$ calculated for each configuration. Successive λ_i values between 0 and 1 should be spaced closely to insure ensemble overlap[81] between neighboring state points. The values of λ_i change the Hamiltonian by perturbing the force field parameters of a subset of solvent molecules ($\lambda_i = 0$) to transform them into additive molecules ($\lambda_i = 1$).

We note that for other additives, where direct mapping of hard-core repulsions is not possible, the linear interpolation presented in Eq. (4) may need to be replaced with a different scheme for better efficiency. Also note that alchemical free energy perturbation techniques where a molecule is "grown" in the solution will fail for ΔF_{nuc} calculations. The initial stage of growth by insertion is a ghost molecule that does not interact with the nucleus at all. As a result the ghost molecule can diffuse into the nucleus, and as the interactions are turned on, it will become an interstitial defect. Additionally, changing solvent (water) molecules into additive molecules may cause a small change in the concentration of solute molecules in solution.

III. CORRECTION FOR FINITE SIZE EFFECTS

The polar γ-glycine crystal has a substantial dipole perpendicular to its charged (001) and (00$\bar{1}$) faces. As a result the γ-glycine nuclei in this study exhibit substantial long-range electrostatic interactions with their own periodic images in a finite simulation box. The required simulation box size to nullify the importance of the long-range dipole-dipole interactions is computationally impractical as illustrated below.

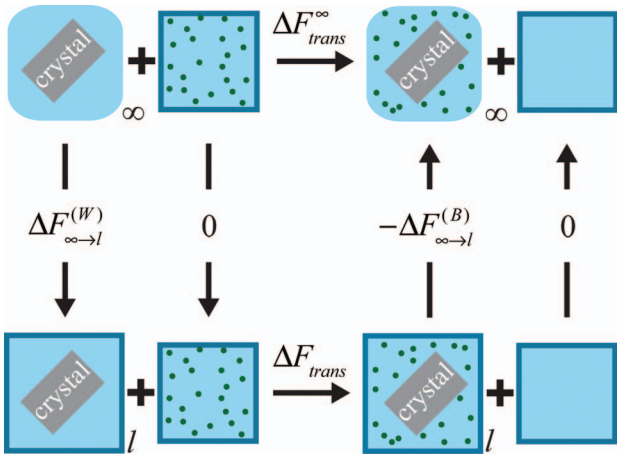

FIG. 2. Thermodynamic cycle to account for self-interactions. Light blue represents solvent, and green points represent additive molecules. The dark blue boxes represent finite simulation boxes with periodic boundary conditions, while boxes with curved corners represent idealized infinite systems with no electrostatic self-interactions.

Instead, we propose a thermodynamic cycle to correct for the finite size self-interactions in Fig. 2.

The transfer free energy for an isolated nucleus, i.e., corrected to remove effects of a finite simulation box, is

$$\Delta F^{\infty}_{trans} = \Delta F^{(W)}_{\infty\to\ell} + \Delta F_{trans} - \Delta F^{(B)}_{\infty\to\ell}, \tag{6}$$

where $\Delta F^{(W)}_{\infty\to\ell}$ and $\Delta F^{(B)}_{\infty\to\ell}$ are the work (per nucleus) to bring an infinite periodic array of nuclei from an infinite separation to a finite separation ℓ for the ΔF_{trans} calculation in water (W) and brine (B) solutions, respectively. Using $\Delta F^{\infty}_{trans}$ in Eq. (2) gives $\Delta\gamma_{\infty}$, the effective change in interfacial free energy for an isolated nucleus. When nuclei do not have long range interactions, $\Delta F^{\infty}_{trans}$ is equivalent to ΔF_{trans}. In our calculation (Sec. V), the nuclei do have long range electrostatic interactions with their own images in water, but not in brine. The dissolved Na^+ and Cl^- ions screen the dipole-dipole interactions. The calculations of $\Delta F^{(W)}_{\infty\to\ell}$ and $\Delta F^{(B)}_{\infty\to\ell}$ depend on the solvent dielectric, on the salt concentration, on nucleus geometry, and on the periodic simulation box dimensions. The calculation is performed quantitatively for specific system parameters in Sec. V.

IV. COMPUTATIONAL DETAILS

Molecular dynamics (MD) simulations of glycine nuclei were performed to analyze the effects of NaCl on the structure and interfacial free energy of α- and γ-glycine nuclei in aqueous solution. Glycine, which exists as a zwitterion in its crystal structure and in neutral solution, was modeled using the Amber force field[82] as modified by Price *et al.*[43] The parameters for the amine, carboxylate, and α-carbon group of glycine zwitterion were taken from the N-terminal glycine, C-terminal glycine, and glycine residues in the Amber force field.[82] The charge on the α-carbon atom was modified slightly to ensure charge neutrality for the glycine molecule.[43] Water is modeled using the TIP3P water model,[79] and ions are modeled using the parameters of Joung and Cheatham optimized for the TIP3P water model.[83]

MD simulations were carried out with NAMD 2.8[84] in the isothermal-isobaric ensemble at 298.15 K and 1 atm with periodic boundary conditions. A Langevin thermostat with a damping coefficient of 5 ps^{-1} was used to control the temperature while pressure was regulated using the Nose-Hoover Langevin piston approach.[85–87] Non-bonded interactions were terminated with a switching function between 11 and 12 Å. Electrostatics interactions were calculated using Particle Mesh Ewald.[88] The bonds in the TIP3P water molecules were constrained using the SETTLE algorithm.[89] A 1 fs time step was used for all simulations.

A. Structural effects of NaCl on nuclei

Simulations of unconstrained seeded α- and γ-glycine nuclei in aqueous glycine solution with and without NaCl were performed to explore the effects of NaCl on the structure of glycine nuclei. Glycine nuclei were initiated as $10 \times 5 \times 10$ unit cells of α-glycine, and $8 \times 8 \times 10$ unit cells of γ-glycine corresponding to cell vectors of at least 50 Å. The crystallites were constructed to give similar sizes and compact shapes for each of the two polymorphs. Unit cell structures were taken from works by Langan *et al.*[90] and Kvick[91] for α-glycine and γ-glycine, respectively. The glycine nuclei were solvated by a supersaturated aqueous glycine solution of 300 mg glycine/ml water. Simulations with NaCl were performed with 80 mg NaCl/ml water, an NaCl concentration at which γ-glycine forms in experimental crystallizations.[37] Note that the solubility of each polymorph changes upon addition of salt to the surrounding solution,[92] but neither nucleus can fully dissolve in the small solvent volume. The simulation boxes were cubic with average box lengths of at least 114 Å and 120 Å for α- and γ-glycine simulation boxes, respectively. This allows for at least 60 Å between images of crystalline glycine nuclei. The glycine nuclei were initially constrained to their crystallographic structure with a harmonic potential of 375 kJ/Å^2 while the solvent was allowed to equilibrated around the nucleus for 5 ns. The harmonic constraints were then removed and whole system was allowed to equilibrate for an additional 5 ns. A production MD trajectory was then run for 10 ns.

Structural changes in the nuclei upon addition of salt were examined using local order parameters.[39,42,93] Specifically, we used RMSD local order parameters which can clearly distinguish and classify molecules in α-glycine, β-glycine, γ-glycine, amorphous, and solution environments.[42] To also identify nuclei with amorphous or surface-melted regions, we identify nuclei, irrespective of crystalline order, as clusters of glycine with high local density.[42] Local density at the ith glycine molecule was defined as the concentration within a cutoff radius $r_c = 6$ Å:

$$\rho(i) = \left(4\pi r_c^3/3\right)^{-1} \sum_{j\neq i} h[r_c - r_{ij}], \tag{7}$$

where r_{ij} is the distance between the centroids of glycine molecules i and j, and $h[x]$ is the Heaviside function: $h[x] = 1$ for $x > 0$ and $h[x] = 0$, otherwise.[42] The glycine nucleus is identified by clustering glycine molecules within 6 Å of each other when both neighbors exceed the local threshold

density $\rho(i) > 6.63/\text{nm}^3$. This threshold density corresponds to at least 6 molecules within r_c. Details on the RMSD order parameters and justification for the chosen cutoffs is available in our previous work.[42] The RMSD local order parameter analysis was performed for MD trajectories of unconstrained α- and γ-glycine nuclei in aqueous solution with and without NaCl.

B. Effects of NaCl on interfacial free energy

The change in interfacial free energy upon NaCl addition, $\Delta\gamma$, for α- and γ-glycine nuclei was calculated using an alchemical solvent transformation. ΔF_{trans} was calculated from Eq. (3) with separate alchemical solvent transformations to obtain both ΔF_{nuc} and ΔF_{soln}. The simulation box for computing ΔF_{nuc} was prepared by solvating nuclei carved from an equilibrated and minimized bulk crystal structure. The α- and γ-glycine nuclei were made up of $5 \times 2 \times 5$, and $4 \times 4 \times 5$ unit cells, giving cell vectors of approximately 26 Å. The nuclei have volumes 15440 Å^3 and 17520 Å^3 for α- and γ-glycine, respectively. The sizes of the nuclei in this study are subcritical, meaning that they would redissolve if left unconstrained. (The glycine solutions are near saturation, so there is little driving force for growth.) To prevent nuclei from redissolving, the atoms in glycine nuclei are constrained with a harmonic potential of 1050 kJ/Å^2. Because of the constraints, the $\Delta\gamma$ calculation reflects only the initially exposed faces. The α-glycine nuclei were placed in a cubic simulation box of length 55.3 ± 0.1 Å and the γ-glycine nuclei were placed in a cubic simulation box of length 60.5 ± 0.1 Å. The nuclei were rotated such that the (010) face of α-glycine and the (001) face of γ-glycine were perpendicular to the $\langle 111 \rangle$ vector in the simulation box. The fixed orientation maximizes the distance between charged faces on the (001) and (00$\bar{1}$) faces of γ-glycine, and therefore minimizes the electrostatic self-interaction. The distance between periodic images of glycine nuclei was at least 24 Å while the distance between parallel (010) and (0$\bar{1}$0) faces of α-glycine was 71.9 ± 0.3 Å and the distance between parallel (001) and (00$\bar{1}$) faces of γ-glycine was 77.5 ± 0.3 Å. The solution concentration of the $\lambda = 0$ state point was 293 mg glycine/ml water (3.33 ± 0.02 M). After a subset of the water molecules are transformed into Na^+ or Cl^-, the solution concentration at $\lambda = 1$ is 300 mg glycine/ml H_2O, and 80 mg NaCl/ml water (or 3.36 ± 0.02 M and 1.16 ± 0.01 M concentration of glycine and NaCl, respectively). The ΔF_{soln} simulation boxes necessarily used solution concentrations identical to the ΔF_{nuc} simulations. The ΔF_{soln} simulation box contains less solution with only 30 NaCl ion pairs, as compared to 109 and 141 in the α- and γ-glycine ΔF_{nuc} simulation boxes. When calculating ΔF_{trans}, the value of ΔF_{soln} must be scaled accordingly.

Many state points, i.e., λ values, were required for convergence in the computation of ΔF_{soln} and ΔF_{nuc}. The total number of state points was 214, 378, and 463 for solution, α-glycine, and γ-glycine, respectively. For each FEP calculation, the initial condition was created from the final molecular configuration of a 2 ns MD trajectory in the $\lambda = 0$ state. Each state point was then equilibrated during a 1 ns MD trajectory. The averages in Eq. (5) were then computed using configurations taken every 100 fs along an additional 1 ns MD trajectory.

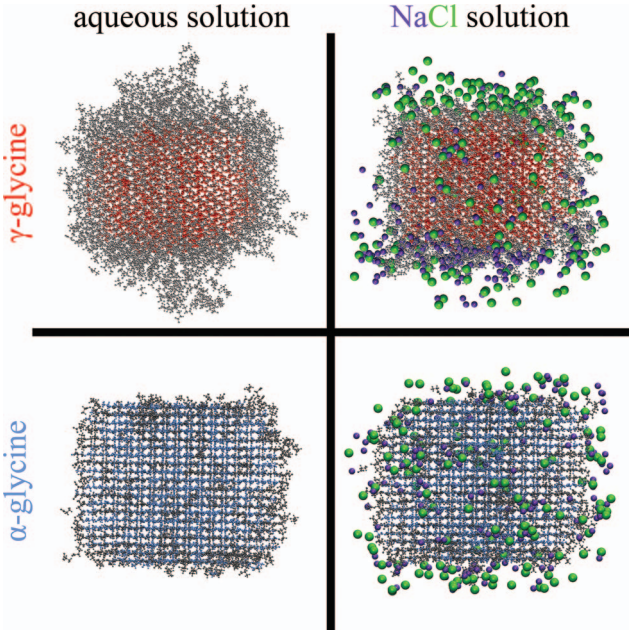

FIG. 3. Unconstrained glycine nuclei in aqueous and NaCl solutions. The water and glycine molecules in the surrounding solution are removed for clarity and to reveal the locations of Na^+ and Cl^- ions. Glycine molecules with α-glycine, and γ-glycine structure are colored blue and red, respectively. Glycine molecules that are amorphous (i.e., not structured like either glycine polymorph) are colored gray. Na^+ are colored purple and Cl^- are colored green. The exposed faces for γ-glycine are ($\bar{1}$00) on the left and (0$\bar{1}$0) on the right with (100) on the top and ($\bar{1}$00) on the bottom. For α-glycine the exposed faces are (001) on the left and (100) on the right with (010) on the top and (0$\bar{1}$0) on the bottom.

V. RESULTS

In Fig. 3, the glycine molecules are colored based on local structure with blue, red, and gray representing α-glycine, γ-glycine, and amorphous glycine respectively. The γ-glycine nucleus in aqueous solution has a core of crystalline glycine surrounded by an amorphous glycine cloud. The amorphous glycine appears to be more prominent around the charged (001) and (00$\bar{1}$) faces of the γ-glycine nucleus, i.e., the top and bottom of faces of the γ-glycine nuclei in Fig. 3. When the glycine nucleus is instead placed in NaCl solution the amorphous layer of glycine is eliminated as the Na^+ and Cl^- ions form a double layer around the charged faces. The structure of the nonpolar α-glycine nucleus in aqueous solution is not visibly affected by the addition of Na^+ and Cl^- ions.

Figure 4 shows a measure of crystallinity within the glycine nuclei: n_{cryst}/n where n_{cryst} is the largest crystalline nucleus within the nucleus (based on the local density cutoff) of size n. The α-glycine and the γ-glycine nuclei in NaCl solution have a similar degree of crystalline order. On the other hand, the γ-glycine nucleus in aqueous solution is substantially less crystalline than the α-glycine nucleus.

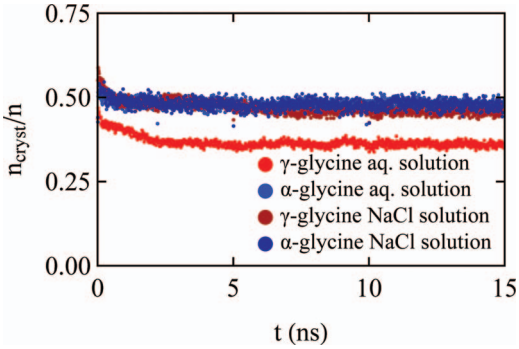

FIG. 4. Crystallinity of α- and γ-glycine nuclei in aqueous solutions and in aqueous NaCl solution.

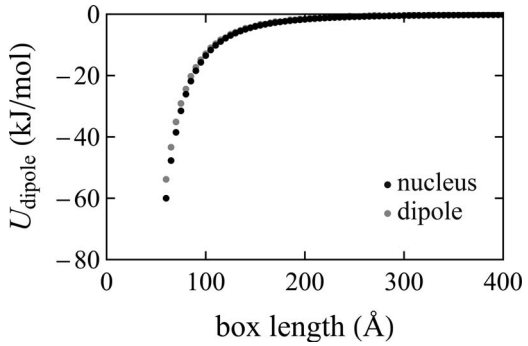

FIG. 5. Electrostatic self-interactions for a γ-glycine nucleus and dipole self-interaction approximation as a function of box length, both using the dielectric of $\epsilon = 105$.

Alchemical solvent transformations were used to compute $\Delta\gamma$, the interfacial free energy changes upon addition of NaCl. This calculation was performed for both polymorphs giving $\Delta\gamma$ for α-glycine ($\Delta\gamma_\alpha$) and $\Delta\gamma$ for γ-glycine nuclei ($\Delta\gamma_\gamma$). The calculation of $\Delta\gamma$ depends on the shape of the nucleus, since the calculated $\Delta\gamma$ is an effective average of the nucleus facets. The nuclei we simulate are compact multiples of unit cells as described in Sec. IV. The values of ΔF_{trans} without finite size effect corrections are summarized in Table I.

The calculations of $\Delta F^{(B)}_{\infty\to\ell}$ and $\Delta F^{(W)}_{\infty\to\ell}$ require a consideration of solvent dielectric constants and Debye lengths. The dielectric constant at a temperature of 298 K was measured by Chaudhari *et al.*[94] for aqueous glycine solutions up to concentrations of 1 M glycine. The supersaturated glycine concentrations in our simulations are approximately 3.3 M, so an extrapolation is necessary. A best-fit line for the data from Chaudhari *et al.* gives $\varepsilon = 79.08 + 22.74 \cdot$ [glycine]/M. Similar lines have been reported for more dilute glycine solutions by Oster *et al.*[95] Direct application of the best fit line from Chaudhuri *et al.* would give $\varepsilon = 154$ when [glycine] $= 3.3$ M. However, the data from Chaudhuri *et al.* at 0.6 M, 0.8 M, and 1.0 M suggest a leveling-off in the concentration dependence of the dielectric constant.[94] The dielectric of pure solid glycine does return to a low value of $\varepsilon \approx 2.5$.[96] This was reported for the γ-glycine polymorph which has a molecular weight and density giving a solid concentration of approximately 22 M. We therefore took the leveling-off in the last data points of Chaudhuri *et al.* to be physical and adopted $\varepsilon = 105$ for 3.3 M glycine solutions. Zwitterions do not contribute to the ionic strength,[97] so the ionic strength and Debye length are easily calculated.

In the brine solution, the Debye length is $\lambda_D = 0.327$ nm which is seven times smaller than the smallest separation distance between γ-glycine nuclei. Therefore, $\Delta F^{(B)}_{\infty\to\ell}$ is negligible for γ-glycine nuclei in the brine solution. Because all surfaces of α-glycine are uncharged, the finite size effects for α-glycine are negligible with and without NaCl in solution. The self-interaction correction for γ-glycine in water, $\Delta F^{(W)}_{\infty\to\ell}$, can be done by approximating the γ-glycine nucleus as a dipole or by using Ewald summation with implicit dielectric solvent in an MD package. The work to bring periodic images of glycine nuclei together is defined as

$$\Delta F^{(W)}_{\infty\to\ell} = U[\ell] - U[\infty], \tag{8}$$

where U is the electrostatic potential energy, and ℓ is the length of the periodic box in the simulation. There are no rotational or translational degrees of freedom to contribute entropy. The objective is to analyze an isolated solute using the simulation machinery for periodic boundary conditions. Figure 5 shows a plot of dipole-dipole interaction energy for the γ-glycine nucleus and an approximation of a γ-glycine nucleus as a dipole in an implicit solvent with the dielectric constant of water at 298.15 K. From Fig. 5, $\Delta F^{(W)}_{\infty\to\ell} = -60.0$ kJ/mol for the γ-glycine nucleus. Details of these calculations are available in the supplementary material.[98]

ΔF_{trans} for α- and γ-glycine nuclei and their component values ΔF_{nuc} and ΔF_{soln} are summarized in Table I. The $\Delta\gamma$ values from ΔF_{trans} as well as the finite size corrected $\Delta\gamma$ are also listed in Table I. The errors in ΔF_{nuc} and ΔF_{soln} are calculated using the ParseFEP package[99] in VMD.[100] The errors in ΔF_{nuc} and ΔF_{soln} resulting from a limited number of stages in the free energy perturbation are small, no more than 1 kJ/mol.

The addition of NaCl causes the effective interfacial free energy of the α-glycine nucleus to *increase* by 3.1 mJ/m^2 while *decreasing* the interfacial free energy of the γ-glycine nucleus by 7.7 mJ/m^2. Increases in the interfacial free energy lead to an increased nucleation barrier and decreased nucleation rate. Therefore, the calculations presented here support the experimental results that α-glycine nucleates out of water solution while salt lowers the barrier and increases the rate of γ-glycine nucleation. Beyond simple agreement with the net change in effective interfacial free energy between α- and γ-glycine nuclei, $\Delta\gamma$ for each nucleus is also in agreement with experimental findings. Since α-glycine nucleates faster out of aqueous solution, than γ-glycine from brine solution,[56]

TABLE I. Summary of results for the calculations of $\Delta\gamma_\alpha$ and $\Delta\gamma_\gamma$.

	α-glycine nucleus	γ-glycine nucleus
ΔF_{trans}/(kJ/mol)	69 ± 1.3	-136 ± 1.4
$\Delta\gamma_\ell$/(mJ/m^2)	3.1 ± 0.1	-5.3 ± 0.1
$\Delta\gamma_\infty$/(mJ/m^2)	3.1 ± 0.1	-7.7 ± 0.1
$\Delta\gamma_{D-H}$/(mJ/m^2)	...	-65.3

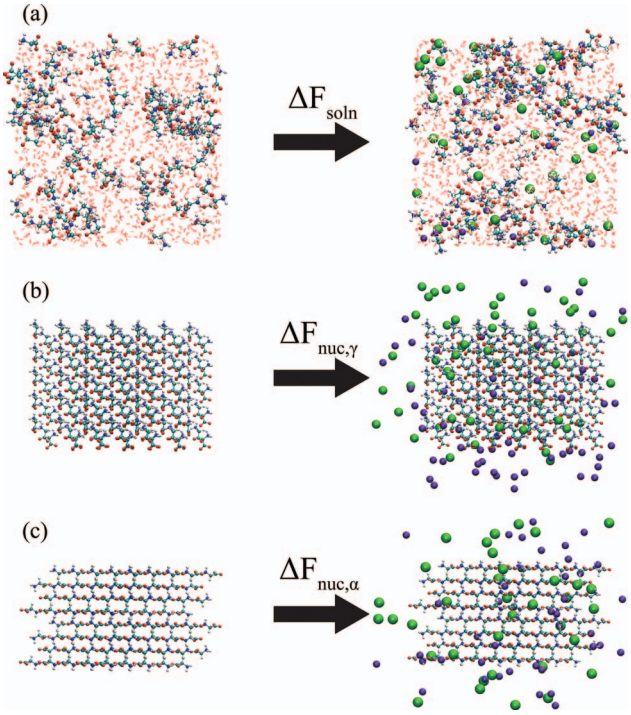

FIG. 6. Simulation snapshots of solution and glycine nuclei from calculation of ΔF_{soln}, $\Delta F_{nuc,\gamma}$, and $\Delta F_{nuc,\alpha}$. Solution molecules are removed from (b) and (c) for clarity. The color scheme differs from that in Fig. 3 because the nuclei are restrained to α or γ structures, and cannot form a melted layer. Hydrogen, nitrogen, carbon, and oxygen atoms are colored white, blue, cyan, and red, respectively.

NaCl must encourage the formation of γ-glycine while suppressing the formation of α-glycine in aqueous NaCl solution. Simulation snapshots from the ΔF_{trans} calculation are shown in Fig. 6. As was seen in the case of the unconstrained nuclei shown in Fig. 3, the strong dipole in the γ-glycine nucleus leads to the formation of a double layer by Na^+ and Cl^- around the (001) and $(00\bar{1})$ faces. Since the γ-glycine nuclei are constrained, their surface is unable to restructure in aqueous solution. α-glycine lacks a net surface charge on any of its faces, so the ions do not form a double layer. However, ions can interact strongly with local areas of positive and negative charge. As a result, ions can disrupt the bonding of glycine molecules to the nucleus, potentially leading to the observed increase in interfacial free energy. Although surface melting of γ-glycine may play an important role in polymorph selection, interactions of the Na^+ and Cl^- with the glycine nuclei are also important.

VI. DEBYE-HÜCKEL ESTIMATE OF $\Delta\gamma_\gamma$

$\Delta\gamma_\gamma$ for the constrained polar γ-glycine nucleus can be qualitatively predicted from Debye-Hückel theory. A simple Debye-Hückel estimate for $\Delta\gamma$ can be derived by assuming the nucleus is a sphere with a polarized surface charge distribution. The charge distribution on the surface of a polarized sphere of radius R is

$$\sigma = \sigma_{max}\cos\theta \tag{9}$$

where σ_{max} is the maximum surface charge density at the two polar ends of the nucleus, i.e., at $\theta = 0$ and $\theta = \pi$. The Debye-Hückel equation for the electrostatic potential Φ is

$$\nabla^2\Phi = \lambda_D^{-2}\Phi, \tag{10}$$

where $\lambda_D = (\epsilon k_B T/2e^2 c_\pm)^{1/2}$ is the Debye length. Equation (10) can be solved by separation of variables or an eigenfunction expansion. A general solution that vanishes infinitely far from the nucleus and which has azimuthal symmetry can be obtained in terms of Legendre polynomials and modified spherical Bessel functions. Details of the solution are given in the supplementary material.[98] The boundary condition at the surface of the nucleus is

$$\epsilon\frac{\partial\Phi}{\partial r}\bigg|_{r=R} = -\sigma_{max}\cos\theta. \tag{11}$$

The boundary condition in Eq. (11) eliminates all but one term in the spherical harmonic expansion and gives

$$\Phi(r,\theta) = \frac{\sigma_{max}R^3(1+r/\lambda_D)exp[-(r-R)/\lambda_D]\cos\theta}{\epsilon\left(2+2R/\lambda_D+R^2/\lambda_D^2\right)r^2}. \tag{12}$$

Equation (12) shows that both the surface potential $\Phi(R,\theta)$ and also the range of the potential depend on λ_D. Specifically, at the positively charged north pole, $\Phi(R,0) = \sigma_{max}R(1+R/\lambda_D)/[\epsilon(2+2R/\lambda_D+R^2/\lambda_D^2)$. The potential at locations away from the surface can be normalized by the maximum surface potential $\Phi(R,0)$ to separately reveal how the range depends on λ_D:

$$\frac{\Phi(r,\theta)}{\Phi(R,0)} = \frac{R^2(1+r/\lambda_D)}{r^2(1+R/\lambda_D)}exp[-(r-R)/\lambda_D]\cos\theta. \tag{13}$$

In the absence of salt, the Debye length is much greater than the nucleus size, $\lambda_D \gg R$, but the unscreened potential remains short ranged because of its dipolar origin. Figure 7 shows $\Phi(r,\theta)/\Phi(R,0)$ in the limit $\lambda_D/R \to \infty$ and for the case $\lambda_D/R = 0.15$.

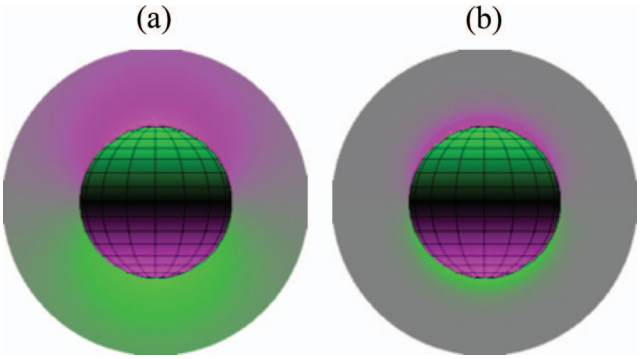

FIG. 7. The electrostatic potential around a polar spherical nucleus of radius 18.4 Å (a) in aqueous solution, and (b) in brine with 80 mg NaCl/ml water. Around the nucleus, green regions have positive potential, purple regions have negative potential, and gray regions are at zero potential. The surface of the nucleus is also colored from green to purple according to the surface charge density.

With the electrostatic potential $\Phi(r, \theta)$ we can calculate the electrostatic free energy using[101]

$$F = \frac{1}{2}\int \rho_f \Phi d\mathbf{r}, \tag{14}$$

where ρ_f is the fixed charge density. Equation (9) for the surface charge density can equivalently be written as a volume charge density $\rho_f = \sigma_{max}\delta[r - R]\cos\theta$ for use in Eq. (14). Contributions due to the mobile charges cancel with the entropy terms in the linearized form of the electrostatic free energy. The integral can be evaluated

$$F = \frac{\pi\sigma_{max}^2 R^3(1 + R/\lambda_D)}{\epsilon\left(1 + R/\lambda_D + R^2/2\lambda_D^2\right)}. \tag{15}$$

Therefore, the Debye-Hückel theory predicts that the free energy per unit area of a polar nucleus with radius R changes upon salt addition by $\Delta\gamma = [F(R/\lambda_D) - F(0)]/4\pi R^2$, or

$$\Delta\gamma_{D-H} = -\frac{\sigma_{max}^2 R}{4\epsilon}\left\{\frac{R^2/2\lambda_D^2}{1 + R/\lambda_D + R^2/2\lambda_D^2}\right\}, \tag{16}$$

where the subscript D-H stands for Debye-Hückel. Using $\epsilon = 105\varepsilon_0$ and [NaCl] = 1.16 ± 0.01 M, i.e., the salt concentration in the alchemical transformation calculations, gives $\lambda_D = 3.27$ Å. The sphere is assumed to have a radius of $R = 18.4$ Å which gives a surface area equal to that of the constrained γ-glycine nucleus. Setting $\sigma_{max} = 0.027$ e/Å^2 makes the dipole moment of the sphere the same as that of the γ-glycine nucleus in the simulations. Inserting these values gives $R/\lambda_D = 5.05$ and $\Delta\gamma_{D-H} = -65.3$ mJ/m^2.

The Debye-Hückel theory correctly predicts an interfacial energy reduction, but $\Delta\gamma_{D-H}$ is much larger than the estimate obtained from the simulations (−7.7 mJ/m^2). Note that the NaCl concentration required to favor γ-glycine nucleation is quite high (1.16 M), while Debye-Hückel theory is quantitatively valid only for low salt concentrations (∼0.01 M). Additionally, Debye-Hückel theory requires the dimensionless potential to be everywhere smaller than unity. The dimensionless surface potential near the poles of the γ-nucleus is ±4.9 at the high salt concentration and even higher without salt. Debye-Hückel theory also cannot account for changes in interfacial free energy that result from the "short-wavelength" variations in surface charge on α-glycine. In the case of α-glycine, the alchemical transformation route to $\Delta\gamma_\alpha$ shows an increase of 3.1 mJ/m^2. Because surfaces of α-glycine carry no net charge Debye-Hückel theory would predict $\Delta\gamma_\alpha = 0$, or perhaps a slightly negative value because of molecular scale modulation of the surface charge density. Debye-Hückel theory also fails to anticipate some interactions which emerge from divalent salts,[102,103] and these may be important for some nucleation processes. For example, Towler *et al.* obtained γ-glycine with NaCl and α-glycine with $Mg(NO_3)_2$, $MgSO_4$, and $Ca(NO_3)_2$ all at the same ionic strength.[36]

For all of the above reasons, one might anticipate a failure of the linear Debye-Hückel theory in the present application. However, the nonlinear Poisson-Boltzmann equation also seems to perform badly. A flat-plane approximation to the geometry is approximately justified at the high salt condition because $\lambda_D \ll R$. Using the one-dimensional solution to the Poisson-Boltzmann equation[104] on the charged surfaces of the nucleus gives a modestly better estimate, $\Delta\gamma_\gamma = -40$ mJ/m^2. The value $\Delta\gamma_\gamma = -40$ mJ/m^2 was obtained as an average over two charged surfaces and four charge-neutral surfaces of a polarized cubic nucleus. Note that this calculation still uses Debye-Hückel for the zero-salt condition because nonlinear terms in the electrostatics calculation vanish in the absence of salt. The Poisson-Boltzmann calculation demonstrates that the discrepancy between alchemical solvent transformation results and the Debye-Hückel estimate is not entirely due to nonlinearity.[103]

We therefore conclude that the alchemical transformation results, while far more difficult to obtain, are more correct. Experimental measurement of nucleation rates shows that the nucleation rate of γ-glycine in brine solution is slower than the nucleation rate of α-glycine in water.[56] Furthermore, the nucleation rate of γ-glycine in brine must exceed the nucleation rate of α-glycine in brine. Specifically, experiments suggest the inequalities $J(\alpha, \text{brine}) < J(\gamma, \text{brine}) < J(\alpha, \text{water})$. From these reports, we see that NaCl causes a decrease in the nucleation rate of α-glycine and presumably NaCl causes an increase in the nucleation rate of γ-glycine. The effect of salt on γ-glycine nuclei could have been anticipated, but the effect on α-glycine is not a priori obvious.

VII. CONCLUSIONS

We have studied the effects of the additive NaCl on the structure and interfacial energy of α- and γ-glycine nuclei in aqueous solution. Using RMSD local order parameters we analyzed the effects of Na^+ and Cl^- on the structure of α- and γ-glycine nuclei in solution. The γ-glycine nucleus in aqueous solution develops a melted layer of amorphous glycine around the nucleus. When NaCl is present, the ions form a double layer, stabilizing the polar glycine polymorph and eliminating the surface melted layer. α-glycine lacks charged faces so the α-glycine structure is largely unaffected by the addition of NaCl. To quantify the stabilizing effect of NaCl on γ-glycine nuclei, we introduced an alchemical transformation approach to change the aqueous solution of glycine into a brine solution of glycine. The alchemical transformation is performed both with and without a nucleus in solution, and for nuclei of α-glycine and γ-glycine polymorphs. The calculations quantify the change in the effective interfacial free energy due to the NaCl additive. Our calculations show that adding 80 mg NaCl/ml water reduces the interfacial free energy of a γ-glycine nucleus by 7.7 mJ/m^2 and increases the effective interfacial free energy of an α-glycine nucleus by 3.1 mJ/m^2. The result for γ-glycine is consistent with experiments which observe γ-glycine nucleation from brine solution, but never from pure aqueous solution. Additionally, the prediction that salt retards α-glycine nucleation is consistent with experimental reports on nucleation rates which suggest: $J(\alpha, \text{brine}) < J(\gamma, \text{brine}) < J(\alpha, \text{water})$.[56] Our results for γ-glycine nuclei are qualitatively consistent with Debye-Hückel theory and Poisson-Boltzmann theory, but both of these methods badly overestimate the change in interfacial free energy. Only the alchemical solvent transformation approach was able to predict the effect of salt on both

polar and non-polar polymorphs. Quantitative predictions will likely depend on the facets exposed on the restrained nucleus, and on the choice of forcefield. However, the results from this study suggest a general "salting out" strategy for obtaining the polar polymorph. It will be interesting to test this strategy for obtaining the polar polymorphs of other molecules.[105–109] The alchemical transformation method may also help understand the effects of other solvent additives on interfacial free energies during nucleation.

ACKNOWLEDGMENTS

Nathan Duff was supported by the Institute for Multiscale Materials Simulations at the Los Alamos National Lab. Baron Peters was supported by NSF CAREER Award No. 0955502. Jeremy D. Schmit and Yuba Raj Dahal were supported by Kansas State University startup funds. Computational resources were provided by the Center for Scientific Computing at the CNSI and MRL: NSF MRSEC (DMR-1121053) and NSF CNS-0960316. Additional computational resources were provided by the Extreme Science and Engineering Discovery Environment (XSEDE), which is supported by National Science Foundation Grant No. OCI-1053575. We thank Daniel Hooks for stimulating discussions.

[1] J. Chen, B. Sarma, J. M. B. Evans, and A. S. Myerson, "Pharmaceutical crystallization," Cryst. Growth Des. **11**, 887–895 (2011).
[2] A. Llinas and J. M. Goodman, "Polymorph control: Past, present and future," Drug Discovery Today **13**, 198–210 (2008).
[3] M. A. Lovette, A. R. Browning, D. W. Griffin, J. P. Sizemore, R. C. Snyder, and M. F. Doherty, "Crystal shape engineering," Ind. Eng. Chem. Res. **47**, 9812–9833 (2008).
[4] S. L. Price, "Computed crystal energy landscapes for understanding and predicting organic crystal structures and polymorphism," Acc. Chem. Res. **42**, 117–126 (2009).
[5] J. Aaltonen, M. Alleso, S. Mirza, V. Koradia, K. C. Gordon, and J. Rantanen, "Solid form screening-a review," Eur. J. Pharm. Biopharm. **71**, 23–37 (2009).
[6] L. Addadi, S. Raz, and S. Weiner, "Taking advantage of disorder: Amorphous calcium carbonate and its roles in biomineralization," Adv. Mater. **15**, 959–970 (2003).
[7] D. Gebauer and H. Colfen, "Prenucleation clusters and non-classical nucleation," Nano Today **6**, 564–584 (2011).
[8] T. Kovács, F. C. Meldrum, and H. K. Christenson, "Crystal nucleation without supersaturation," J. Phys. Chem. Lett. **3**, 1602–1606 (2012).
[9] J. Kawano, N. Shimobayashi, A. Miyake, and M. Kitamura, "Precipitation diagram of calcium carbonate polymorphs: Its construction and significance," J. Phys. Condens. Matter **21**, 425102 (2009).
[10] P. Raiteri, R. Demichelis, J. D. Gale, M. Kellermeier, D. Gebauer, D. Quigley, L. B. Wright, and T. R. Walsh, "Exploring the influence of organic species on pre- and post-nucleation calcium carbonate," Faraday Discuss. **159**, 61 (2012).
[11] R. Schulman and E. Winfree, "Synthesis of crystals with a programmable kinetic barrier to nucleation," Proc. Natl. Acad. Sci. U.S.A. **104**, 15236–15241 (2007).
[12] W. L. Miller and A. Cacciuto, "Exploiting classical nucleation theory for reverse self-assembly," J. Chem. Phys. **133**, 234108 (2010).
[13] L. O. Hedges and S. Whitelam, "Limit of validity of Ostwald's rule of stages in a statistical mechanical model of crystallization," J. Chem. Phys. **135**, 164902 (2011).
[14] J. Bernstein, "Polymorphism-A Perspective," Cryst. Growth Des. **11**, 632–650 (2011).
[15] D. Braga, F. Grepioni, and L. Maini, "The growing world of crystal forms," Chem. Commun. **46**, 6232–6242 (2010).
[16] R. J. Davey and N. Blagden, "Polymorphism in molecular crystals: Stabilization of a metastable form by conformational mimicry," J. Am. Chem. Soc. **119**, 1767–1772 (1997).
[17] W. Ostwald, "Studies on the formation and transformation of solid bodies," Z. Phys. Chem. **22**, 289–330 (1987).
[18] R. J. Davey, "Solvent effects in crystallization processes," in *Current Topics in Materials Science*, edited by E. Kaldis (North-Holland, Amsterdam, Netherlands, 1982), Vol. 8, pp. 429–479.
[19] R. C. Kelly and N. Rodriguez-Hornedo, "Solvent effects on the crystallization and preferential nucleation of carbamazepine anhydrous polymorphs: A molecular recognition perspective," Org. Process Res. Dev. **13**, 1291–1300 (2009).
[20] S. A. Kulkarni, E. S. McGarrity, H. Meekes, and J. H. ter Horst, "Isonicotinamide self-association: The link between solvent and polymorph nucleation," Chem. Commun. **48**, 4983–4985 (2012).
[21] M. Svärd and A. C. Rasmuson, "m-Hydroxybenzoic acid: Quantifying thermodynamic stability and influence of solvent on the nucleation of a polymorphic system," Cryst. Growth Des. **13**, 1140–1152 (2013).
[22] I. N. Stranski and D. Totomanow, "Velocity of nucleus formation and Ostwald's step rule," Z. Phys. Chem. **163**, 399–408 (1933).
[23] B. Peters, "Competing nucleation pathways in a mixture of oppositely charged colloids: Out-of-equilibrium nucleation revisited," J. Chem. Phys. **131**, 244103 (2009).
[24] A. Nangia, "Conformational polymorphism in organic crystals," Acc. Chem. Res. **41**, 595–604 (2008).
[25] M. Kitamura, "Strategy for control of crystallization of polymorphs," Cryst. Eng. Comm. **11**, 949 (2009).
[26] L. Derdour, C. Sivakumar, D. Skliar, S. K. Pack, C. J. Lai, J. P. Vernille, and S. Kiang, "Crystallization from solutions containing multiple conformers. 2. Experimental study and model validation," Cryst. Growth Des. **12**, 5188–5196 (2012).
[27] L. Yu, G. A. Stephenson, C. A. Mitchell, C. A. Bunnell, S. V. Snorek, J. J. Bowyer, T. B. Borchardt, J. G. Stowell, and S. R. Byrn, "Thermochemistry and conformational polymorphism of a hexamorphic crystal system," J. Am. Chem. Soc. **122**, 585–591 (2000).
[28] K. R. Back, R. J. Davey, T. Grecu, C. A. Hunter, and L. S. Taylor, "Molecular conformation and crystallization: The case of ethenzamide," Cryst. Growth Des. **12**, 6110–6117 (2012).
[29] L. Yu, S. M. Reutzel-Edens, and C. A. Mitchell, "Crystallization and polymorphism of conformationally flexible molecules: Problems, patterns, and strategies," Org. Process Res. Dev. **4**, 396–402 (2000).
[30] J. Anwar, P. K. Boateng, R. Tamaki, and S. Odedra, "Mode of action and design rules for additives that modulate crystal nucleation," Angew. Chem., Int. Ed. **48**, 1596–1600 (2009).
[31] X. Y. Liu, "Interfacial effect of molecules on nucleation kinetics," J. Phys. Chem. B **105**, 11550–11558 (2001).
[32] S. Chattopadhyay, D. Erdemir, J. M. B. Evans, J. Ilavsky, H. Amenitsch, C. U. Segre, and A. S. Myerson, "SAXS study of the nucleation of glycine crystals from a supersaturated solution," Cryst. Growth Des. **5**, 523–527 (2005).
[33] D. Erdemir, S. Chattopadhyay, L. Guo, J. Ilavsky, H. Amenitsch, C. Segre, and A. Myerson, "Relationship between self-association of glycine molecules in supersaturated solutions and solid state outcome," Phys. Rev. Lett. **99**, 115702 (2007).
[34] A. S. Myerson and P. Y. Lo, "Diffusion and cluster formation in supersaturated solutions," J. Cryst. Growth **99**, 1048–1052 (1990).
[35] J. Huang, T. C. Stringfellow, and L. Yu, "Glycine exists mainly as monomers, not dimers, in supersaturated aqueous solutions: Implications for understanding its crystallization and polymorphism," J. Am. Chem. Soc. **130**, 13973–13980 (2008).
[36] C. S. Towler, R. J. Davey, R. W. Lancaster, and C. J. Price, "Impact of molecular speciation on crystal nucleation in polymorphic systems: The conundrum of γ glycine and molecular 'self-poisoning'," J. Am. Chem. Soc. **126**, 13347–13353 (2004).
[37] X. Yang, J. Lu, X.-J. Wang, and C.-B. Ching, "Effect of sodium chloride on the nucleation and polymorphic transformation of glycine," J. Cryst. Growth **310**, 604–611 (2008).
[38] G. Han, P. S. Chow, and R. B. H. Tan, "Direct comparison of α- and γ-glycine growth rates in acidic and basic solutions: New insights into glycine polymorphism," Cryst. Growth Des. **12**, 2213–2220 (2012).
[39] E. E. Santiso and B. L. Trout, "A general set of order parameters for molecular crystals," J. Chem. Phys. **134**, 064109 (2011).
[40] J. Chen and B. L. Trout, "A computational study of the mechanism of the selective crystallization of α- and β-glycine from water and methanol-water mixture," J. Phys. Chem. B **114**, 13764–13772 (2010).

[41]Y. Yani, P. S. Chow, and R. B. H. Tan, "Glycine open dimers in solution: New insights into α-glycine nucleation and growth," Cryst. Growth Des. **12**, 4771–4778 (2012).
[42]N. Duff and B. Peters, "Polymorph specific RMSD local order parameters for molecular crystals and nuclei: α-, β-, and γ-glycine," J. Chem. Phys. **135**, 134101 (2011).
[43]S. L. Price, S. Hamad, A. Torrisi, P. G. Karamertzanis, M. Leslie, and C. R. A. Catlow, "Applications of DL_POLY and DL_MULTI to organic molecular crystals," Mol. Simul. **32**, 985–997 (2006).
[44]S. Hamad, C. E. Hughes, C. R. A. Catlow, and K. D. M. Harris, "Clustering of glycine molecules in aqueous solution studied by molecular dynamics simulation," J. Phys. Chem. B **112**, 7280–7288 (2008).
[45]Y. Iitaka, "The crystal structure of γ-glycine," Acta Crystallogr. **14**, 1–10 (1961).
[46]G. Albrecht and R. B. Corey, "The crystal structure of glycine," J. Am. Chem. Soc. **61**, 1087–1103 (1939).
[47]Y. Iitaka, "Crystal structure of beta-glycine," Nature (London) **183**, 390–391 (1959).
[48]I. Weissbuch, V. Y. Torbeev, L. Leiserowitz, and M. Lahav, "Solvent effect on crystal polymorphism: Why addition of methanol or ethanol to aqueous solutions induces the precipitation of the least stable beta form of glycine," Angew. Chem., Int. Ed. **44**, 3226–3229 (2005).
[49]C. E. Hughes and K. D. M. Harris, "Direct observation of a transient polymorph during crystallization," Chem. Commun. **46**, 4982–4984 (2010).
[50]V. Y. Torbeev, E. Shavit, I. Weissbuch, L. Leiserowitz, and M. Lahav, "Control of crystal polymorphism by tuning the structure of auxiliary molecules as nucleation inhibitors: The beta-polymorph of glycine grown in aqueous solutions," Cryst. Growth Des. **5**, 2190–2196 (2005).
[51]M. N. Bhat and S. M. Dharmaprakash, "Effect of solvents on the growth morphology and physical characteristics of nonlinear optical γ-glycine crystals," J. Cryst. Growth **242**, 245–252 (2002).
[52]M. N. Bhat and S. M. Dharmaprakash, "Growth of nonlinear optical γ-glycine crystals," J. Cryst. Growth **236**, 376–380 (2002).
[53]L. Yu and K. Ng, "Glycine crystallization during spray drying: The pH effect on salt and polymorphic forms," J. Pharm. Sci. **91**, 2367–2375 (2002).
[54]M. Xu and K. D. M. Harris, "Alteration of polymorphic selectivity through different crystallization mechanisms occurring in the same crystallization solution," J. Phys. Chem. B **111**, 8705–8707 (2007).
[55]V. Buch, A. Milet, R. Vácha, P. Jungwirth, and J. P. Devlin, "Water surface is acidic," Proc. Natl. Acad. Sci. U.S.A. **104**, 7342–7347 (2007).
[56]G. Han, S. Thirunahari, P. Shan Chow, and R. B. H. Tan, "Resolving the longstanding riddle of pH-dependent outcome of glycine polymorphic nucleation," Cryst. Eng. Comm. **15**, 1218 (2013).
[57]V. Agarwal and B. Peters, "Solute precipitate nucleation: A review of theory and simulation advances," Adv. Chem. Phys. (in press).
[58]D. Kashchiev, *Nucleation: Basic Theory with Applications* (Butterworth-Heinemann, Oxford, 2000).
[59]P. G. Debenedetti, *Metastable Liquids: Concepts and Principles* (Princeton University Press, Princeton, 1996).
[60]B. Peters, "On the coupling between slow diffusion transport and barrier crossing in nucleation," J. Chem. Phys. **135**, 044107 (2011).
[61]A. Jawor-Baczynska, J. Sefcik, and B. D. Moore, "250 nm glycine-rich nanodroplets are formed on dissolution of glycine crystals but are too small to provide productive nucleation sites," Cryst. Growth Des. **13**, 470–478 (2013).
[62]W. Wu and G. H. Nancollas, "Determination of interfacial tension from crystallization and dissolution data: A comparison with other methods," Adv. Colloid Interface Sci. **79**, 229–279 (1999).
[63]J. N. Israelachvili, *Intermolecular and Surface Forces*, 2nd ed. (Academic Press, San Diego, 1992).
[64]J. Q. Broughton and G. H. Gilmer, "Molecular dynamics investigation of the crystal-fluid interface. IV. Free energies of crystal-vapor systems," J. Chem. Phys. **84**, 5741–5748 (1986).
[65]J. Hoyt, M. Asta, and A. Karma, "Method for computing the anisotropy of the solid-liquid interfacial free energy," Phys. Rev. Lett. **86**, 5530–5533 (2001).
[66]B. B. Laird, R. L. Davidchack, Y. Yang, and M. Asta, "Determination of the solid-liquid interfacial free energy along a coexistence line by Gibbs-Cahn integration," J. Chem. Phys. **131**, 114110 (2009).
[67]S. Angioletti-Uberti, M. Ceriotti, P. D. Lee, and M. W. Finnis, "Solid-liquid interface free energy through metadynamics simulations," Phys. Rev. B **81**, 125416 (2010).
[68]S. Auer and D. Frenkel, "Prediction of absolute crystal nucleation rate in hard-sphere colloids," Nature (London) **409**, 1020 (2001).
[69]C. Valeriani, E. Sanz, and D. Frenkel, "Rate of homogeneous crystal nucleation in molten NaCl," J. Chem. Phys. **122**, 194501 (2005).
[70]N. Duff and B. Peters, "Nucleation in a Potts lattice gas model of crystallization from solution," J. Chem. Phys. **131**, 184101 (2009).
[71]N. Duff and B. Peters, "Mitosis method for directly calculating the interfacial free energy of nuclei," Mol. Simul. **36**, 498–504 (2010).
[72]R. Persson, S. Nordholm, G. Perlovich, and L. Lindfors, "Monte Carlo studies of drug nucleation 1: Formation of crystalline clusters of bicalutamide in water," J. Phys. Chem. B **115**, 3062–3072 (2011).
[73]J. D. Chodera, D. L. Mobley, M. R. Shirts, R. W. Dixon, K. Branson, and V. S. Pande, "Alchemical free energy methods for drug discovery: Progress and challenges," Curr. Opin. Struct. Biol. **21**, 150–160 (2011).
[74]J. Michel and J. W. Essex, "Prediction of protein-ligand binding affinity by free energy simulations: Assumptions, pitfalls and expectations," J. Comput.-Aided Mol. Des. **24**, 639–658 (2010).
[75]C. D. Christ, A. E. Mark, and W. F. van Gunsteren, "Basic ingredients of free energy calculations: A review," J. Comput. Chem. **31**, 1569–1582 (2010).
[76]R. W. Zwanzig, "High-temperature equation of state by a perturbation method. I. Nonpolar gases," J. Chem. Phys. **22**, 1420–1426 (1954).
[77]W. L. Jorgensen and C. Ravimohan, "Monte Carlo simulation of differences in free energies of hydration," J. Chem. Phys. **83**, 3050–3054 (1985).
[78]P. A. Bash, U. C. Singh, F. K. Brown, R. Langridge, and P. K. Kollman, "Calculation of the relative change in binding free energy of a protein-inhibitor complex," Science **235**, 574–576 (1987).
[79]W. L. Jorgensen, J. Chandrasekhar, J. D. Madura, R. W. Impey, and M. L. Klein, "Comparison of simple potential functions for simulating liquid water," J. Chem. Phys. **79**, 926–935 (1983).
[80]C. Chipot, and A. Pohorille, "Calculating free energy differences using perturbation theory," in *Free Energy Calculations*, edited by C. Chipot and A. Pohorille (Springer, Berlin, 2007), Chap. 2.
[81]T. B. Tan, A. J. Schultz, and D. A. Kofke, "Suitability of umbrella- and overlap-sampling methods for calculation of solid-phase free energies by molecular simulation," J. Chem. Phys. **132**, 214103 (2010).
[82]V. Hornak, R. Abel, A. Okur, B. Strockbine, A. Roitberg, and C. Simmerling, "Comparison of multiple Amber force fields and development of improved protein backbone parameters," Proteins: Struct., Funct., Bioinf. **65**, 712–725 (2006).
[83]I. S. Joung and T. E. Cheatham, "Determination of alkali and halide monovalent ion parameters for use in explicitly solvated biomolecular simulations," J. Phys. Chem. B **112**, 9020–9041 (2008).
[84]J. C. Phillips, R. Braun, W. Wang, J. Gumbart, E. Tajkhorshid, E. Villa, C. Chipot, R. D. Skeel, L. Kale, and K. Schulten, "Scalable molecular dynamics with NAMD," J. Comput. Chem. **26**, 1781–1802 (2005).
[85]S. E. Feller, Y. Zhang, R. W. Pastor, and B. R. Brooks, "Constant pressure molecular dynamics simulation: The Langevin piston method," J. Chem. Phys. **103**, 4613–4621 (1995).
[86]G. J. Martyna, D. J. Tobias, and M. L. Klein, "Constant pressure molecular dynamics algorithms," J. Chem. Phys. **101**, 4177–4189 (1994).
[87]D. Quigley and M. I. J. Probert, "Langevin dynamics in constant pressure extended systems," J. Chem. Phys. **120**, 11432–11441 (2004).
[88]T. Darden, D. York, and L. Pedersen, "Particle mesh Ewald: An N log (N) method for Ewald sums in large systems," J. Chem. Phys. **98**, 10089–10092 (1993).
[89]S. Miyamoto and P. A. Kollman, "Settle: An analytical version of the SHAKE and RATTLE algorithm for rigid water models," J. Comput. Chem. **13**, 952–962 (1992).
[90]P. Langan, S. A. Mason, D. Myles, and P. Benno, "Structural characterization of crystals of a-glycine during anomalous electrical behaviour research papers," Acta Crystallogr. B **58**, 728–733 (2002).
[91]A. Kvick, "An experimental study of the influence of temperature on a hydrogen-bonded system: The crystal structure of y glycine at 83K and 298K by neutron diffraction," Acta Crystallogr. B **36**, 115–120 (1980).
[92]A. Bouchard, G. W. Hofland, and G.-J. Witkamp, "Solubility of glycine polymorphs and recrystallization of-glycine," J. Chem. Eng. Data **52**, 1626–1629 (2007).
[93]A. S. Keys, C. R. Iacovella, and S. C. Glotzer, "Characterizing complex particle morphologies through shape matching: Descriptors, applications, and algorithms," J. Comput. Phys. **230**, 6438–6463 (2011).
[94]A. Chaudhari, A. G. Shankarwar, B. R. Arbad, and S. C. Mehrotra, "Dielectric relaxation in glycine-water and glycine-ethanol-water solu-

tions using time domain reflectometry," J. Solution Chem. **33**, 313–322 (2004).
[95]G. Oster, D. Price, L. G. Joyner, and J. G. Kirkwood, "The dielectric constants of solutions of glycine and pyridine betaine in water-dioxane mixtures," J. Am. Chem. Soc. **66**, 946–948 (1944).
[96]M. E. Peter and P. Ramasamy, "Growth of gamma glycine crystal and its characterisation," Spectrochim. Acta, Part A **75**, 1417–1421 (2010).
[97]E. Stellwagen, J. D. Pranter, and N. C. Stellwagen, "Do zwitterions contribute to the ionic strength of a solution?" Anal. Biochem. **373**, 407–409 (2008).
[98]See supplemental material at http://dx.doi.org/10.1063/1.4853775 for details on the Debye-Huckel solution.
[99]P. Liu, F. Dehez, W. Cai, and C. Chipot, "A toolkit for the analysis of free-energy perturbation calculations," J. Chem. Theory Comput. **8**, 2606–2616 (2012).
[100]W. Humphrey, A. Dalke, and K. Schulten, "VMD: Visual molecular dynamics," J. Mol. Graphics **14**, 33–38 (1996).
[101]K. A. Sharp and B. Honig, "Calculating total electrostatic energies with the nonlinear Poisson-Boltzmann equatlon," J. Phys. Chem. **94**, 7684–7692 (1990).
[102]P. Linse, G. Gunnarsson, and B. Jonsson, "Electrostatic interactions in micellar solutions," J. Phys. Chem. **86**, 413–421 (1982).
[103]V. Vlachy, "Ionic effects beyond Poisson-Boltzmann theory," Annu. Rev. Phys. Chem. **50**, 145–165 (1999).
[104]J. D. Schmit, S. Whitelam, and K. Dill, "Electrostatics and aggregation: How charge can turn a crystal into a gel," J. Chem. Phys. **135**, 085103 (2011).
[105]R. Hiremath, S. W. Varney, and J. A. Swift, "Selective growth of a less stable polymorph of 2-iodo-4-nitroaniline on a self-assembled monolayer template," Chem. Commun. **2004**, 2676–2677.
[106]X. Mei and C. Wolf, "Crystallization through slow acid-controlled hydrolytic release of a highly polar organic compound: Formation of a dipolar acridone polymorph," Cryst. Growth Des. **5**, 1667–1670 (2005).
[107]R. C. Hall, I. C. Paul, and D. Y. Curtin, "Structures and interconversion of polymorphs of 2,3-dichloroquinizarin: Use of second harmonic generation to follow the change of a centrosymmetric to a polar structure," J. Am. Chem. Soc. **110**, 2848–2854 (1988).
[108]R. Centore, M. Jazbinsek, A. Tuzi, A. Roviello, A. Capobianco, and A. Peluso, "A series of compounds forming polar crystals and showing single-crystal-to-single-crystal transitions between polar phases," Cryst. Eng. Comm. **14**, 2645 (2012).
[109]C. Stoica, P. Tinnemans, H. Meekes, W. J. P. V. Enckevort, and E. Vlieg, "A series of compounds forming polar crystals and showing single-crystal-to-single-crystal transitions between polar phases," Cryst. Growth Des. **6**, 1311–1317 (2006).